

Phase transition of interfacial water at low-dimensions

Wenlong Liang(梁文龙), Yujie Huang(黄雨婕), Yue Zhang(张悦), and Chunlei Wang(王春雷)
Citation: Chin. Phys. B, 2026, 35 (**2**): 020501. DOI: 10.1088/1674-1056/ae12da
http://cpb.iphy.ac.cn; http://iopscience.iop.org/cpb

What follows is a list of articles you may be interested in

Energy mechanism of the first-order superradiant phase transition in cavity-BEC system with double asymmetric pump beams

Wei Qin(覃威), Dong-Chen Zheng(郑东琛), Jia-Ying Lin(林佳颖), Yuan-Hong Chen(陈元鸿), and Renyuan Liao(廖任远)
Chin. Phys. B, 2025, 34 (**12**): 120507. DOI: 10.1088/1674-1056/addeb7

Four-body interactions in the long-range Hamiltonian mean-field model

Qiang Zhang(张强), Haojie Luo(罗浩杰), Bingling Cen(岑炳玲), and Yu Xue(薛郁)
Chin. Phys. B, 2025, 34 (**11**): 110501. DOI: 10.1088/1674-1056/addccf

Universality of percolation at dynamic pseudocritical point

Qiyuan Shi(石骐源), Shuo Wei(魏硕), Youjin Deng(邓友金), and Ming Li(李明)
Chin. Phys. B, 2025, 34 (**4**): 040501. DOI: 10.1088/1674-1056/adaccf

Stable water droplets on composite structures formed by embedded water into fully hydroxylated *β*-cristobalite silica

Hanqi Gong(龚菡琪), Chonghai Qi(齐崇海), Junwei Yang(杨俊伟), Jige Chen(陈济舸), Xiaoling Lei(雷晓玲), Liang Zhao(赵亮), and Chunlei Wang(王春雷)
Chin. Phys. B, 2021, 30 (**1**): 010503. DOI: 10.1088/1674-1056/abc2b7

Hydrophobic nanochannel self-assembled by amphipathic Janus particles confined in aqueous nano-space

Gang Fang(方钢), Nan Sheng(盛楠), Tan Jin(金坦), Yousheng Xu(许友生), Hai Sun(孙海), Jun Yao(姚军), Wei Zhuang(庄巍), Haiping Fang(方海平)
Chin. Phys. B, 2018, 27 (**3**): 030505. DOI: 10.1088/1674-1056/27/3/030505

TOPICAL REVIEW — A celebration of the 90th Anniversary of the Birth of Bolin Hao

Phase transition of interfacial water at low-dimensions

Wenlong Liang(梁文龙)[1], Yujie Huang(黄雨婕)[1], Yue Zhang(张悦)[1,2], and Chunlei Wang(王春雷)[1,†]

[1] *College of Sciences, Shanghai University, Shanghai* 200444, *China*
[2] *School of Machinery and Automation, Weifang University, Weifang* 261000, *China*

(Received 22 August 2025; revised manuscript received 10 October 2025; accepted manuscript online 14 October 2025)

Water molecules can form hydrogen bonds. At the solid surfaces, the preferential alignment of water molecules due to the heterogeneous atomic distributions can induce ordered hydrogen bond networks of water molecules with spatially heterogeneous patterns and slower dynamics compared to bulk water. Both the confinement and the surface atomic structures can induce the water phase transitions at low dimensional spaces. Here, we review how the phase transitions of interfacial water affect the surface physical behaviors, such as wetting, ice nucleation and the terahertz-wave–water interactions, from solid materials to the biological surfaces. These works help extend our knowledge of the physics properties of the interfacial water, particularly the multi-phase behaviors in materials and biology sciences.

Keywords: interfacial water, ordered water, phase transition, hydrophilicity/hydrophobicity, THz electric waves

PACS: 05.70.–a, 64.60.Q–

DOI: 10.1088/1674-1056/ae12da **CSTR:** 32038.14.CPB.ae12da

1. Introduction

Water has been considered as the salient component in the physical, chemical and biological systems. Phase transitions of water are widespread in natural environments, such as the first-order transition between ice and liquid water,[1] and the liquid transition (LLT) of water,[2,3] which describes the separation of water into two coexisting liquid forms: one with a high-density liquid (HDL)and the other with a low-density liquid (LDL). The interfacial water confined in distinct local environments can display significantly different behaviors from those of bulk water. Gaining a deep insight into solid/liquid interfacial water, particularly at the intersection of solid, liquid, and gas phases, is essential for advancing knowledge across multiple disciplines, such as physical,[4–8] chemical,[9,10] and biological[11–15] processes. Such understanding plays a pivotal role in applications like seawater desalination,[16,17] heterogeneous catalysis,[18–24] geochemical mineral reactions,[25–27] and micro-nanoscale fluid transport devices.[28–30]

Water molecules exhibit stratification phenomena near solid surfaces at low dimensions, where surface–water interactions play a critical role in determining the structure of interfacial water layers. In 2009, we reported an unexpected theoretical prediction: the formation of two-dimensional ordered water monolayer that does not completely wet water at room temperature. This ordered water monolayer exhibited hydrophobic behavior with the water droplets on this monolayer, despite the intrinsically hydrophilic interfaces. The phase transition of interfacial water from a disordered liquid phase to an ordered ice-like phase can be induced by modulating the distribution of positive and negative charges on an ionic substrate. Such ordered ice-like water layers have been observed on a variety of material surfaces, including metals, metal oxides, polymers, and self-assembled monolayers. Similar two-dimensional ice-like water can be found near antifreeze proteins or silver iodide surfaces. Herein, the ordered interfacial water with particular hydrogen-bond network promotes the formation of 3D ice nuclei and significantly lowers the nucleation energy barrier. Physically, the ordered water structures are expected to exhibit characteristic vibrational modes absent in bulk water. By applying external terahertz electromagnetic fields at the specific frequencies, the order–disorder phase transition of interfacial water can be precisely controlled, highlighting terahertz fields as a novel tool for manipulating aqueous phase transitions at interfaces. In this review, we mainly summarize our recent works on the impact of phase transition of water contacting with surface on the surface wetting, ice nucleation and the external terahertz fields–water coupling.

2. Ordered water on the two-dimensional solid materials surfaces

In systems with quasi-one-dimensional confinement, such as carbon nanotubes, a first-order phase transition behavior occurs in confined water and a quasi-one dimensional water chain is formed.[31] The external mechanical or electrical stimuli can induce on–off gating effects of water across the carbon nanotube.[32–34] When water interacts with two-dimensional

†Corresponding author. E-mail: wangchunlei1982@shu.edu.cn

© 2026 Chinese Physical Society and IOP Publishing Ltd. All rights, including for text and data mining, AI training, and similar technologies, are reserved.

surfaces through confinement or adsorption, it tends to exhibit unique structural arrangements and distinctive dynamic behavior. Progress in high-resolution experimental methods has made it possible to observe interfacial water with well-defined phase characteristics. One of the earliest pieces of direct evidence for such ordered water layers under ambient conditions came from studies on mica using atomic force microscopy (AFM) by Hu *et al*.,[35] who pioneeringly captured images of spatially organized water layers on mica. Odelius *et al.*[36] used theoretical modeling to propose that these layers form a two-dimensional hydrogen-bond network lacking free OH terminations. This theoretical insight was later confirmed by Miranda and colleagues using sum-frequency generation (SFG) spectroscopy,[37] supporting the presence of this distinct interfacial structure. The metal surface water structures have attracted extensive attention. Earlier, in 2002, Ogasawara and colleagues experimentally detected ice-like hexagonal layers on Pt(111) after annealing the surface at 140 K,[38] where water molecules retained in-plane hydrogen bonding while adhering to the metal. Water molecules exhibited partial dissociation behavior on Ru(0001).[39] In 2002, Meng *et al*. identified two distinct hydrogen bond strengths within these surface-bound hexagonal water networks.[40] The water molecules phase transition behaviors confined between hydrophobic slip space is of particular interest. In 2009, Debenedetti *et al*.[41] have used molecular dynamics simulations to study the phase transition of water under nanoconfinement between hydrophobic structured walls, where the wall–wall separation distance was the key to understand the phase transition. One study by Han *et al.*[42] involving quasi-two-dimensional hydrophobic slit nanopores suggests the existence of a critical point where continuous and first-order phase transitions intersect.

Recent advancements in high-resolution methods have enabled atomic-scale visualization of interfacial structures on various solid surfaces. Using a combination of electrochemical analysis, *in situ* Raman spectroscopy, and computational modeling, Li *et al*.[9] studied water layers on atomically smooth Pd single-crystal substrates. Their research uncovered highly ordered interfacial water configurations that significantly enhanced electron transfer at the interface, thereby boosting the rate of hydrogen evolution reactions (HER). Jiang *et al*. utilized q-plus mode scanning tunneling microscopy (STM) to uncover previously unobserved structures of interfacial water. In 2014, they employed STM at cryogenic temperatures (5 K) to resolve water tetramers on the NaCl(001) surface.[43] The non-contact atomic force microscopy (AFM) allowed them to capture atomic-scale images of a two-dimensional hexagonal ice lattice on Au(111),[44] shedding light on its edge growth mechanisms. By 2024, they experimentally confirmed superlubricity in low-dimensional hexagonal water layers.[45] In addition, the molecular-resolution mapping of heterogeneous ice nucleation pathways by Wang *et al*., achieved via *in-situ* cryo-TEM, offers direct molecular-level insight.[46]

Computational understanding how water behaves at the molecular scale under extreme confinement is still a formidable task, primarily because of the significant computational cost of precise simulations and the experimental difficulty of accessing nanoscale environments. In light of this, artificial intelligence (AI) has become a transformative tool in molecular-level modeling. A recent study by Michaelides *et al*.[47] employed a hybrid computational strategy to examine monolayer water confined within hydrophobic two-dimensional channels, starting from first-principles. Their methodology integrated the high accuracy of quantum Monte Carlo with the computational efficiency of machine learning potentials (MLPs), enabling a comprehensive structural exploration across diverse temperatures and pressures. Zeng *et al*.[48] have predicted the rich proton dynamics and phase behaviors of nanoconfined ices from large-scale path-integral molecular dynamics simulations and machine learning potential.

It is well established that liquid water typically spreads over itself due to its strong hydrogen-bonding network. In 2009, we made an unexpected theoretical prediction: a water droplet positioned atop a structured monolayer of water at ambient temperature, which we referred to as an "ordered water monolayer that does not completely wet water"[49] (see Fig. 1(a)). The theoretical solid model was composed of a flat hexagonal surface exhibiting an alternating distribution of charges (Figs. 1(b) and 1(c)), where red and blue represented positive and negative sites, respectively. When the surface charge value q was larger than 0.6 e, the water molecules began to form a droplet sitting atop a hexagonally arranged structured monolayer. We further discovered that the ordered structuring of interfacial water is induced only when the distance between positive and negative ions approaches the characteristic oxygen–oxygen distance of stable water dimers ($\sim$ 0.284 nm). Both the charge magnitude of ions and their separation on the ions substrate surface can trigger the transition of interfacial water from a disordered liquid phase to an ordered hexagonal monolayer ice-like structure. This ordered water monolayer is consistent with the low-pressure hexagonal phase predicted by Michaelides *et al*. using first-principles calculations for water confined in graphene slits.[48] However, a key distinction exists: the ordered phase at the interface is stabilized by the specific distribution of positive and negative charges, rather than by spatial confinement, and it remains stable under ambient conditions. In 2019, we identified a sharp phase transition within the interfacial water monolayer, manifested by an abrupt change in interaction energy resulting from minor variations in molecular dipole moment (Fig. 1(d)). This observation provides strong evidence for an

order–disorder transition in two-dimensionally confined interfacial water.[50] The diffusion constant of the ordered water phase ($\mu = 13.6$ D) was measured to be less than half that of the two disordered phases. In contrast, the self-diffusion constant in the second water layer (4 Å $< z \leq$ 7.5 Å) adjacent to the ordered phase was significantly higher than that in the disordered phases (Fig. 1(e)). Furthermore, we systematically examined how variations in ion charge magnitude and inter-ion distance on the substrate regulate the water contact angle on the interfacial monolayer (Fig. 1(f)). A contact angle greater than zero serves as a clear indicator of the presence of the ordered phase.

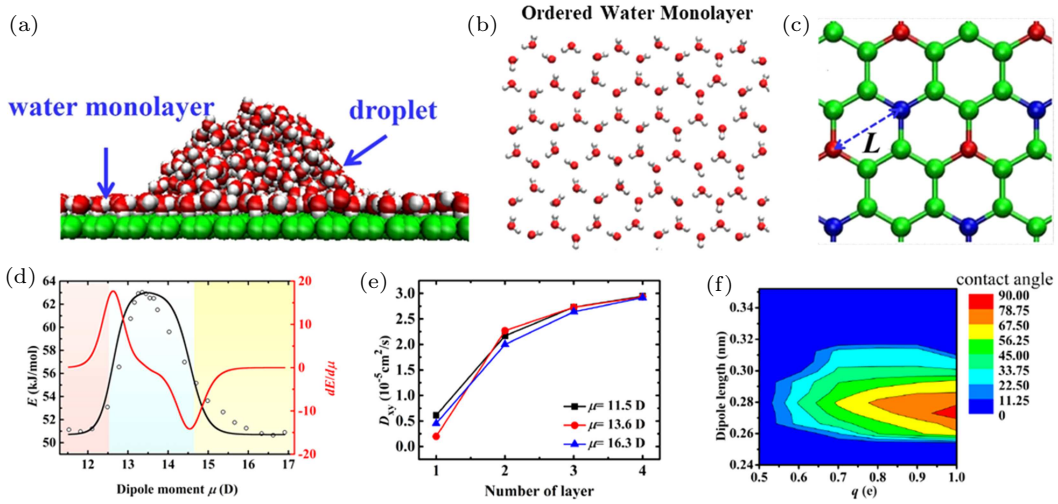


Fig. 1. (a) A stable water droplet coexists with a thin water monolayer absorbed on a modeled solid surface. (b) Ordered water monolayer structure of the first water layer on the hexagonal solid surface when $L = 0.284$ nm and $q = 1.0$ e. (c) Structure of the model solid surface with a hexagonal, charged pattern. Red presents the positive-charged atoms, and the blue presents the negative-charged atoms. (d) Plot of absolute values of attractive interaction energy E of one water molecule in the first water monolayer and its neighboring water molecules in the same monolayer, versus the solid surface dipole moment μ for the system with a 4-nm-thick water film, together with the differentiated values $\mathrm{d}E/\mathrm{d}\mu$ (right red axis). (e) In-plane self-diffusion coefficient (D_{xy}) of water molecules in various layers. (f) Contours of the contact angles of the water droplets on the solid surfaces with different charge values q and bond lengths l.

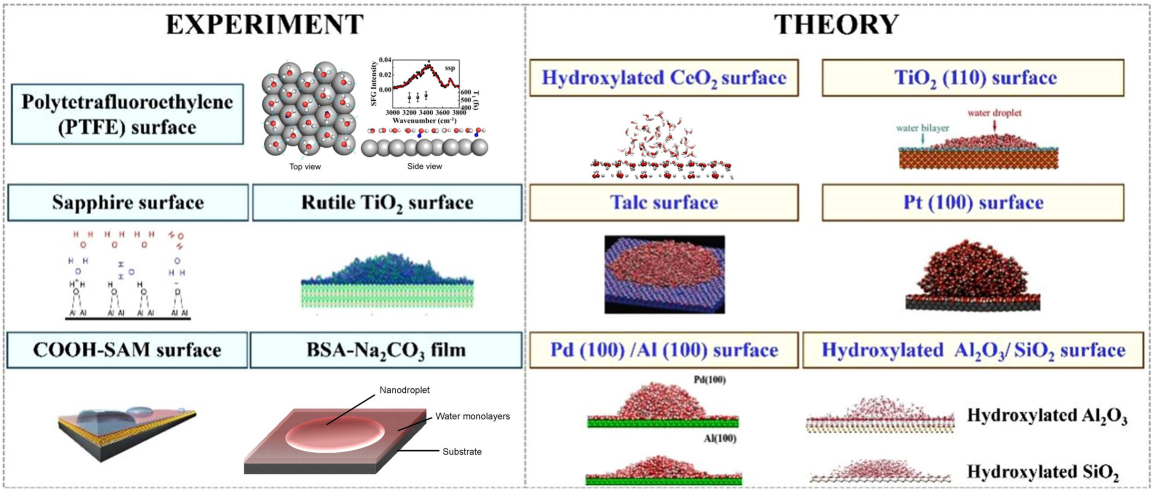


Fig. 2. Summary of recent experimental and theoretical works on the water droplets coexisting with a thin water monolayer absorbed on various solid surfaces.

Our analysis demonstrated that the hydrogen bond network is key to understanding the observed non-wetting phenomenon. Given that a single water molecule can form up to four hydrogen bonds, we quantified the average number of bonds both within the monolayer and between the monolayer and the overlying droplet. A clear trade-off emerged: as the number of hydrogen bonds inside the monolayer increased, the bonding between the layers diminished. This reduction in interfacial bonding strength weakens the adhesion between the droplet and the monolayer, thereby facilitating the stable presence of a water droplet on top of the structured layer.

The idea of an "ordered water monolayer that does not completely wet water" has contributed to resolving long-standing questions about surface wettability. One typical example is the wetting behavior on a self-assembled monolayer with the terminal of COOH.[51] We have found an ordered phase structure of an embedded water-COOH composite, which induces the hydrophobicity of this surface. This

can explain why the water droplets coexisting with few-angstrom-thin water layer on COOH-SAM can be experimentally observed.[52] Another notable example is the TiO_2 that has sparked debates regarding its hydrophilic versus hydrophobic nature for decades. Investigations using sum-frequency generation (SFG) spectroscopy, alongside molecular dynamics simulations, we have uncovered well-ordered water arrangements on metal oxide surfaces such as TiO_2.[53] More recently, *ab initio* molecular dynamics simulations have indicated that similar hydrophobic effects may also appear at the interface between water and rare-earth oxides like CeO_2,[54] expanding current insight into interfacial water phenomena.

This line of research has prompted numerous subsequent studies (Fig. 2). For instance, a number of researchers have reported comparable non-wetting phenomena induced by structured monolayers on a variety of substrates, including Pt(100),[55] Pd(100),[56] hydroxylated alumina (a soil constituent),[57] hydroxylated CeO_2,[54] BAS-$NaCO_3$ membrane,[58] talc minerals,[59] and polytetrafluoroethylene (PTFE).[60] These results show that the presence of ordered interfacial water layers that do not completely wet may be a widely occurring trait across different solid surfaces.

3. Water–ice phase transitions at the biological and solid surfaces

To survive in cold environments, nature has endowed various organisms with antifreeze proteins (AFPs), enabling them to thrive under subzero conditions.[61–64] AFPs can bind to ice crystals via their ice-binding surface (IBS). Due to the Kelvin effect, this binding alters the curvature of the ice surface between adjacent AFPs, effectively lowering the freezing point of ice.[65–67] By leveraging nanoscale thermal hysteresis and specific ice-binding, AFPs effectively modulate ice nucleation and growth. These remarkable capabilities underpin their significant potential in applications such as food preservation and cryopreservation.[68–70] Experimental studies have also reported the "Janus effect" of AFPs, where the IBS can promote ice nucleation in supercooled solutions,[71,72] which may exhibit detrimental effects in tissues cryopreservation. The structural rearrangement of water molecules at interfaces gives rise to behaviors that differ significantly from those in bulk water.[73–75] This interfacial restructuring plays a critical role in heterogeneous ice nucleation (HIN), a process widely observed in nature and highly relevant to fields ranging from cloud physics to the food industry.[76–78]

A precise atomic-scale understanding of heterogeneous ice nucleation is essential for distinguishing how AFP surfaces either facilitate or inhibit ice formation. Molinero *et al*. propose that both ice-nucleating proteins (INPs) and AFPs identify ice through diverse anchored clathrate and ice-like motifs.[79] However, their subsequent work challenges the conventional view by demonstrating that interfacial water preordering is not required for AFP ice recognition. Instead, their findings reveal that the protein undergoes rotational diffusion (tumbling) as it approaches the ice surface, only stabilizing when it achieves the optimal orientation and proximity to form the anchored clathrate (AC) motif. They suggest that preordering may arise only on the extensive ice-binding surfaces of aggregated INPs, where it could facilitate nucleation. The simulations in this study were conducted using the rigid, non-polarizable TIP4P/2005 water model, consequently omitting potential polarization effects that could influence protein–ice interactions.[80] Molecular dynamics simulations[81,82] and terahertz experiments[83] show that AFPs create a quasi-ice-like layer in the hydration water on their IBS. A similar ordered layer exists at the ice-water interface. According to the "zipper-like" mechanism, these two ordered layers merge and subsequently crystallize into ice, thereby incorporating the protein into the ice crystal. A recent review[84] demonstrates that forming a quasi-ice-like hydration structure on the IBS is a general characteristic of antifreeze proteins. This suggests that AFP binding to ice is mediated by the structural complementarity between this ordered hydration shell and the similar quasi-liquid layer present on the ice surface. Understanding the dynamical correlation between a protein and its hydration waters is essential to unravel how protein–water interactions trigger biological function.

In 2016, our work[72] demonstrated that different surface regions of AFPs exhibit a Janus-like influence on ice formation: the non-ice-binding face (NIBF) inhibits nucleation, whereas the ice-binding face (IBF) enhances crystal growth. Nucleation temperatures were used to track the freezing events of droplets in contact with NIBF and IBF surfaces (Fig. 3(a)). As seen in Fig. 3(b), when AFP surface coverage remained below 80%, nucleation on the NIBF held steady around -28.0 °C, suggesting minimal inhibitory effect at low interfacial density. A sudden shift occurred at the 80% threshold, where nucleation temperature dropped sharply, indicating the onset of NIBF's suppressive function. This effect saturated at 90% coverage, stabilizing the temperature at -31.9 °C. In contrast, Fig. 3(c) shows that the IBF surface promoted nucleation. At coverage levels under 64%, freezing temperatures hovered around -27.5 °C. Once IBF surface density exceeded 80%, the ice nucleation temperature rapidly rose by approximately 4.5 °C, eventually leveling at -23.0 °C. This sharp rise suggests that dense IBF coverage effectively templates ice nucleation. Our data suggest that the contrasting structural organization of water at NIBF and IBF surfaces — disordered at NIBF versus ordered, ice-like at IBF (Fig. 3(d)) — accounts for their distinct roles in nucleation behavior.

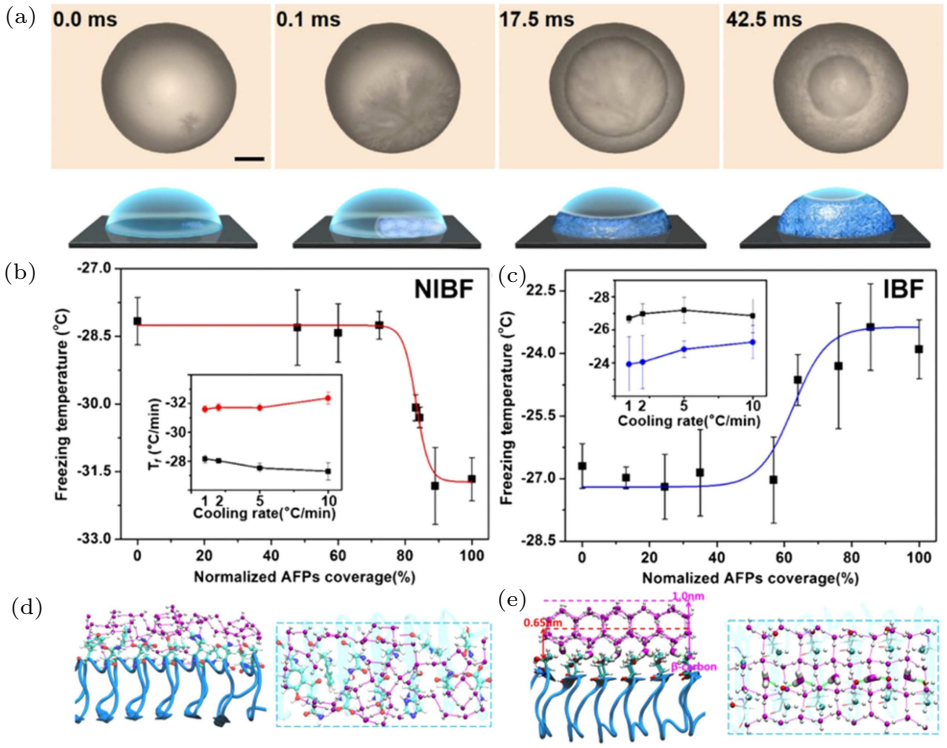


Fig. 3. Ice nucleation behavior on NIBF and IBF surfaces. (a) The top panel displays a representative freezing event of water droplets placed on NIBF and IBF surfaces, captured using a high-speed camera in conjunction with an optical microscope. The bottom panel offers a schematic representation of the corresponding freezing process. Ice nucleation initiates at the interface between the solid surface and the droplet, followed by upward ice growth. Scale bar: 200 μm. (b), (c) Influence of NIBF and IBF on the ice nucleation process. The inset graphs in (b) and (c) depict the nucleation temperatures on fully coated NIBF and IBF surfaces under varying cooling rates, demonstrating that NIBF inhibits the development of a stable ice nucleus while IBF promotes its formation. Approximately 100 separate nucleation events were recorded under consistent treatment conditions, and Gaussian fitting was applied to extract the mean values and standard deviations. (d), (e) Molecular insights into AFP-mediated ice nucleation regulation. The IBF region is shown with hexagonal, ice-like water molecules (magenta-white spheres), along with entrapped water molecules (magenta-white sticks), arranged above IBF sites featuring methyl (cyan-white) and hydroxyl (red-white) groups.

Understanding ice nucleation at the atomic scale has long been a significant challenge in computational chemistry, primarily due to the difficulty of capturing the critical nucleus size. Despite these challenges, molecular dynamics (MD) simulations based on fully atomistic water models can offer more precise insights into the molecular-level interactions between water and proteins, as well as the dynamics of ice formation. Although coarse-grained models such as the mW water model[85–87] have been applied to explore nucleation near protein surfaces and organic monolayers, there remains a gap in achieving atomic-level resolution and mechanistic clarity.

A precise atomic-scale understanding of heterogeneous ice nucleation is essential for distinguishing how AFP surfaces either facilitate or inhibit ice formation. Our recent all-atom molecular dynamics simulations[88] shed light on the stepwise process of pre-critical ice nucleus development on the IBF. The formation sequence begins with one-dimensional (1D) water chains confined within IBF surface grooves, progresses into a two-dimensional (2D) ice-like nano-layer, and eventually transforms into a full three-dimensional (3D) nucleus. In the early stage, single-file water molecules form within the IBF groove, establishing hydrogen bonds with threonine hydroxyl and cysteine carbonyl groups (Fig. 4(a)). These confined waters align along the x-direction with ~ 0.45 nm spacing comparable to the lattice constant of ice Ih and exhibit stable dipole orientations near 90°, indicating highly ordered alignment (Figs. 4(b) and 4(c)). Next, a 2D crystalline water layer appears on the IBF surface, enabled by the TxT motif, whose hydroxyl group spacings ($a_{\mathrm{OH}} \approx 0.74$ nm; $b_{\mathrm{OH}} \approx 0.46$ nm) closely match the lattice spacing of ice ($a_{\mathrm{ice}} \approx 0.73$ nm; $b_{\mathrm{ice}} \approx 0.45$ nm) (Figs. 4(d)–4(f)). This structural compatibility allows both the IBF and confined waters to participate as hydrogen bond donors and acceptors, promoting the assembly of hexagonal water rings. Within each ring, half of the molecules interact directly with the surface or confined water, while the others bridge neighboring water molecules (Fig. 4(d)), ultimately stabilizing the growth of a 3D nucleus (Figs. 4(g) and 4(h)). Importantly, no ice nucleation was observed on the non-ice-binding surface (NIBS), consistent with prior experiments illustrating the Janus-like behavior of AFPs. This comparison underscores the critical influence of surface structural features on nucleation initiation.

Ice nucleation, the initial phase transition during freezing, is described by classical nucleation theory (CNT),[89] which states that crystallization only begins once a stable ice nucleus surpasses a specific free energy barrier. Molec-

ular dynamics trajectories revealed that ice nuclei with fewer than 40 water molecules fluctuated in size (Fig. 5(a)), while those exceeding 50 molecules grew steadily. To pinpoint the critical size, four nuclei around $n \sim 40$ (sizes ~ 28, ~ 38, ~ 40, and ~ 50) were selected for further analysis (Fig. 5(b)). The critical ice nucleus size was determined to be approximately 38 water molecules significantly smaller than the ~ 80 molecules required for homogeneous nucleation at the same temperature.[90] The free energy barrier at 240 K is markedly lower than the 33.2 kJ/mol value characteristic of homogeneous nucleation in Fig. 5(c). More specifically, the associated free energy barriers were analyzed to further clarify the enhancement efficiency of ice nucleation at different temperatures, as seen in Fig. 5(c). We characterized the ability of IBS to lower the critical free energy barrier by $f = G^*_{\mathrm{Het}}/G^*_{\mathrm{Hom}}$. Our study reveals that IBS catalyze ice nucleation by significantly lowering the energetic and structural barriers for phase transition. Simulation results reveal that TmAFP demonstrates pronounced functionality at low temperatures. Specifically, under the 240 K condition, the IBF organizes water molecules into ice-like configurations, leading to a reduction of more than one order of magnitude in activation energy compared to homogeneous nucleation. Such a drastic reduction highlights the catalytic role of the IBF, which organizes water molecules into ice-like structures through hydrogen bonding and geometric alignment. This structural templating facilitates the formation of three-dimensional ice nuclei by minimizing the thermodynamic cost, thus accelerating the freezing process. These insights provide a molecular-level explanation for how antifreeze proteins enhance ice nucleation control.

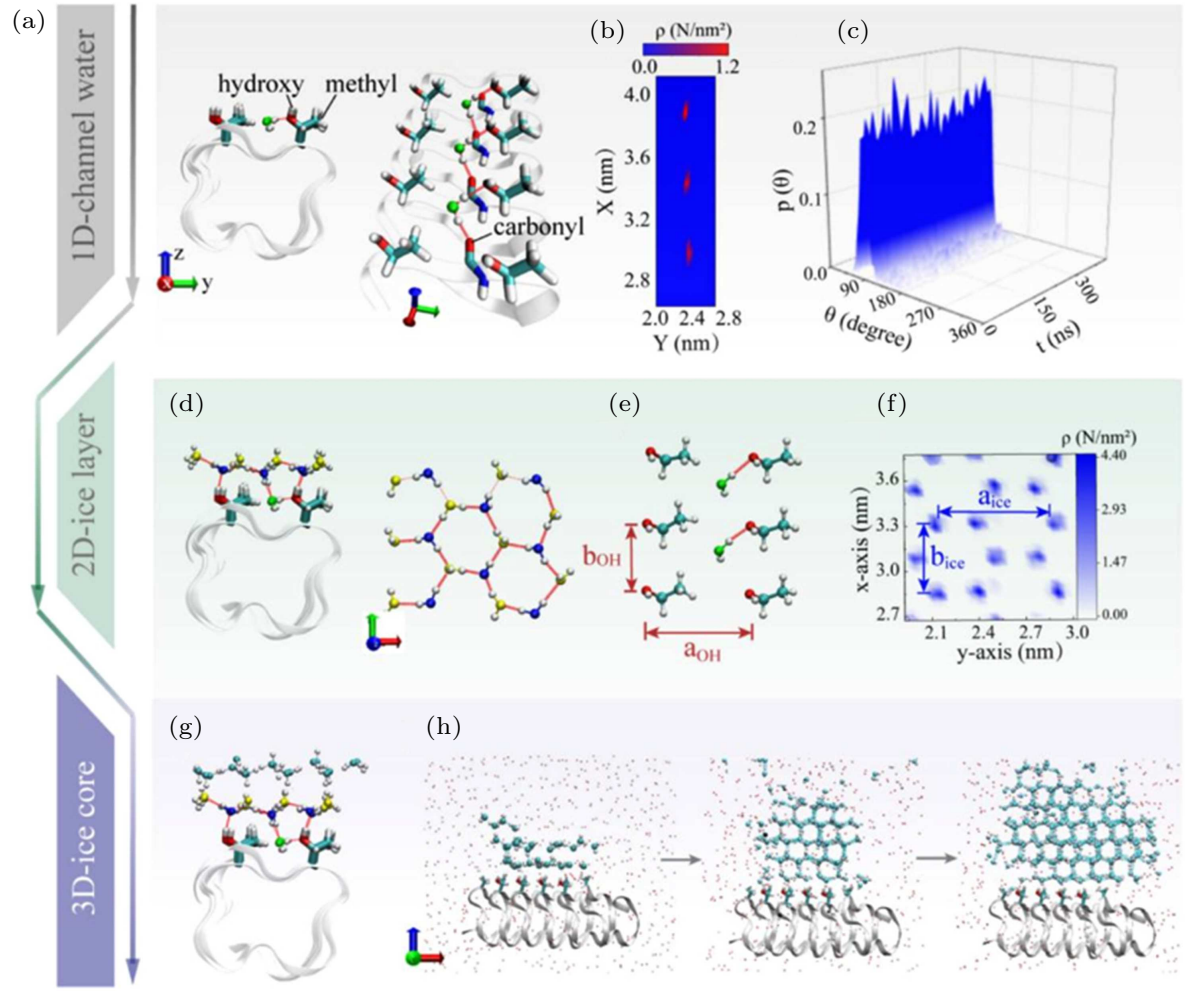


Fig. 4. Simulation-based evidence of ice nucleation at the ice-binding surface (IBS) of TmAFP. (a) Both side and top perspectives reveal confined water (CW) stabilized within a reversed groove framed by threonine residues. These water molecules establish hydrogen bonds with threonine's hydroxyl groups and cysteine's carbonyl groups. The central backbone of the protein is displayed as a silver cartoon, while functional moieties on the IBS are illustrated as colorful sticks. Red dashed lines indicate hydrogen bonding interactions. (b) Spatial density map of confined water projected onto the *xy* plane during microsecond-scale simulations. (c) Time evolution of dipole angle distributions for confined water. The dipole orientation angle (θ) is defined as the angle between each water molecule's dipole moment and the *x*-axis. (d) Snapshots from the side and top views show a structured, ice-like water layer adhered to the IBS, where blue-white and yellow-white spheres represent ice-like water molecules in contact with the protein. (e) Hydroxyl group alignments at the IBS mimic the spatial pattern of ice lattices. (f) This is further supported by the in-plane density map of the ice-like layer relative to the IBS. (g) A new layer of ice begins to grow on top of the first ice-like layer. (h) This development continues, eventually forming a three-dimensional ice nanocrystal. Red spheres represent water in the liquid phase, while blue-white spheres mark water in solid, ice-like states.

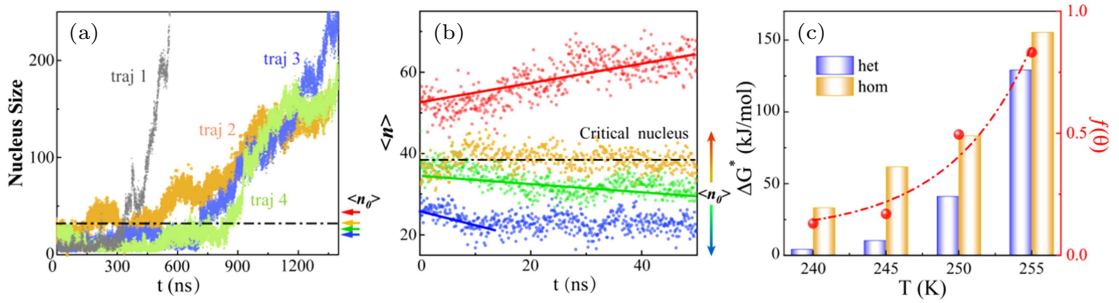


Fig. 5. Exploration of the critical nucleus size and free energy barrier. (a) The nucleus size (number of water molecules in the largest ice nucleus) versus the simulation time in four independent MD simulation trajectories. (b) Nucleus size averaged over 20 independent simulations versus the simulation time. Note that the initial nucleus sizes, $\langle n_0 \rangle$, as marked by the four different colored arrows in (a), were obtained from the four origin MD trajectories. (c) The classical nucleation theory (CNT) prediction, regarding the influence of TmAFP on lowering the nucleation barrier, and the potency factor f of heterogeneous nucleation relative to homogeneous nucleation versus temperature (the dashed line represents the nonlinear polynomial curve fitting).

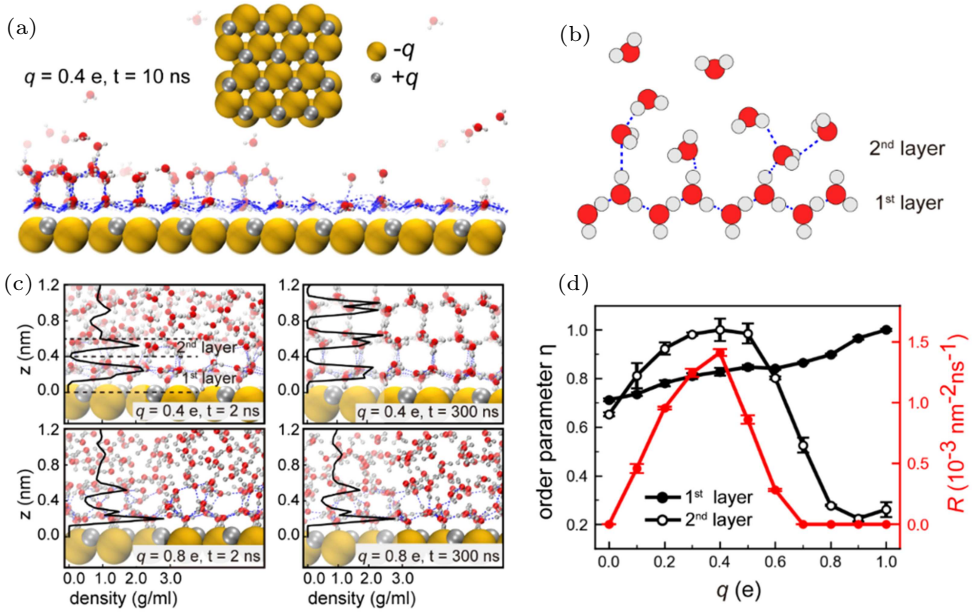


Fig. 6. Ice nucleation process. (a) A representative simulation snapshot illustrates the onset of ice formation on a surface carrying a charge density of $q = 0.4\ e$. The inset displays the atomic structure of the underlying model substrate. (b) Water density distributions and accompanying simulation snapshots highlight the differences in interfacial water organization on surfaces with $q = 0.4\ e$ and $0.8\ e$, evaluated both during the supercooled regime (averaged over 2–3 ns) and at the later stages of freezing or non-freezing (collected from 299–300 ns). (c) A conceptual diagram outlines the sequential freezing process, beginning with the first hydration layer, followed by the second. (d) Ice nucleation rate (R) is shown for 11 different surface models with surface charge magnitudes ranging from 0.0 to 1.0 e, along with corresponding structural order parameters (η) of the first and second hydration layers.

Similarly, in non-biological systems, solid surfaces, such as minerals or engineered materials, can either promote or inhibit ice nucleation depending on their wettability,[91,92] lattice structure,[73] and surface topography.[93,94] For instance, studies have reported distinct interfacial water structures associated with hydrophilic and hydrophobic surfaces, which can influence the freezing behavior of overlying water and the pattern of ice crystal growth.[95,96] However, wettability alone is not a reliable predictor of ice nucleating ability, as it can be affected by factors such as surface morphology and crystallinity.[73,92,97,98] Using the coarse-grained mW water model, Michaelides and colleagues[73] identified three key interfacial scenarios in which water molecules participate in nucleation: (1) formation of the first overlayer of water, (2) construction of the first two overlayers, and (3) promotion of nucleation in upper layers without in-plane templating. This enhanced nucleation requires surfaces with strong water adsorption energy. Furthermore, by applying deep learning techniques, they were able to predict ice-nucleating ability based on structural images of the first water layer.[99] Zhou *et al.* proposed that the ice-nucleation capability of a surface is primarily governed by its average adsorption energy when the surface lattice mismatches ice, whereas for lattice-matched surfaces, the detailed nature of water–surface interactions serves as the key regulatory factor.[100] In addition, they studied ice nucleation on nanopatterned surfaces with alternating hydrophobic and hydrophilic regions. They found that nucleation preferentially occurs within individual patches rather than across boundaries, due to a higher free energy barrier associated with interfacial crossing.[101] The "ice-matching pattern," characterized by ice-like ordering in the dense interfacial water layer, is considered a key attribute of efficient ice nucleators.[92] A

representative example has been observed on the (0001) surface of silver iodide (AgI),[102] where a chair-like conformation is induced in the adjacent water layers closely resembling the layered structure found in bulk ice (hexagonal or cubic). Our recent MD simulations[103] have unveiled fresh perspectives on the phase transition behavior of interfacial water interacting with solid substrates (Fig. 6). By employing a model surface inspired by β-AgI (0001), we observed that although the first hydration layer tends to adopt an ice-like hexagonal hydrogen-bonded arrangement under appropriate surface polarity, it is the second hydration layer that critically governs the transition toward bulk ice. This second layer serves as a structural mediator, connecting the surface-bound ordered water with the surrounding liquid phase, and facilitates the development of a more extensive ice bilayer. Notably, the structural coherence of this intermediate layer shows a strong correlation with the surface's capacity to induce ice formation, and serves as a more reliable indicator than traditional measures like wettability or first-layer structuring. Sun *et al.* simulated heterogeneous ice nucleation on a simple cubic substrate with tunable hydrophilicity and obtained consistent conclusions.[104] These insights refresh the conceptual framework of ice templating from a two-dimensional interface toward a fully three-dimensional model, enhancing our understanding of interfacial phase transitions and offering practical implications for applications in cryopreservation, atmospheric modeling, and anti-icing surface engineering. Moreover, it is well established that interfacial water exhibits pronounced stratification phenomena regardless of whether the substrate is hydrophilic or hydrophobic. While solid–water interactions predominantly govern the structural arrangement of the first water monolayer, their specific mechanistic roles in regulating the phase transition dynamics of water/ice monolayers will be systematically investigated in our study.

4. THz electric waves induce ordered/disordered water transitions

The transition between ordered and disordered states of interfacial water plays a pivotal role in altering surface wettability and the ice nucleation at the macroscopic level. However, the accurate, long-distance and reversible modulation on this surface water is lacking. Water, as a polar molecule, tends to form quasi-one-dimensional or two-dimensional ordered configurations when confined in low-dimensional environments. These ordered structures exhibit distinct resonance characteristics, which span a broad spectral range-from O–H stretching and intermolecular hydrogen bond vibrations to rotational and librational modes. As a result, they display rich spectral responses in the infrared, far-infrared, and terahertz (THz) regions.[105–107]

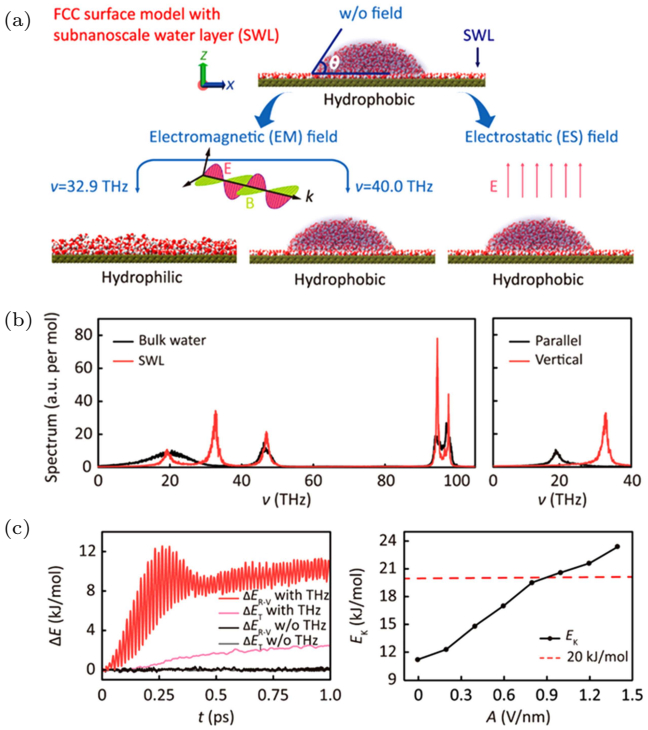


Fig. 7. Terahertz electromagnetic field stimulation drives wetting state transitions of water droplets. (a) The contact angle (θ) of a water droplet responds differently under various electromagnetic field conditions. Without any field applied, the droplet exhibits a hydrophobic state. However, exposure to a 32.9 THz electromagnetic field results in a transition to a superhydrophilic wetting behavior. In contrast, stimulation using either a 40 THz field or a static electric field leads to negligible change in the contact angle. (b) The absorption spectrum comparison between the water monolayer and bulk water (left) reveals a pronounced absorption peak centered at 32.9 THz for the monolayer. This spectral feature arises from the out-of-plane vibrational mode of water molecules perpendicular to the surface (right). (c) The change in rotational–vibrational ($\Delta E_{\mathrm{R-V}}$) and translational (ΔE_{T}) kinetic energies per water molecule in SWL was compared to that with and without the application of 32.9 THz EM stimulus. (d) The total kinetic energy (E_{K}) per molecule of water in SWL at various strengths of 32.9 THz EM stimulus. When the E_{K} value is comparable to the H-bond energy of the water molecule ($\sim$ 20 kJ/mol), the structure of SWL is disrupted, causing the wetting-state transition.

The THz waves, spanning frequencies from 0.1 THz to 100 THz, lie between the infrared and microwave regions. For a long time, progress in this frequency range lagged behind other parts of the electromagnetic spectrum due to the lack of suitable THz sources and detectors — hence it has often been referred to as the "terahertz gap." Interestingly, many key substances in water and biological systems exhibit strong absorption peaks in the THz to mid- and far-infrared regions. As a result, this spectral range has been hailed by NASA as a technological bridge to the future and the "light of life."[108–111] In recent years, significant breakthroughs have been made in the generation of high-power THz radiation. Techniques such as optical rectification,[112] linear accelerators,[113] and laser-driven ion sources[114] have enabled THz instruments to achieve extremely high field strengths, typically exceeding 1 MV/cm and reaching tens of MV/cm under specific conditions. Traditionally, bulk water has been known to strongly absorb THz waves across a broad frequency range

(with bandwidths exceeding 1000 cm^{-1}), owing to its complex hydrogen-bond network and the strong coupling between hydrogen bonds and librational motions of water molecules.

The unique "fingerprint" vibrational spectra of interfacial ordered water provide opportunities for frequency-specific external fields to modulate molecular dynamics such as rotational and vibrational motions. By analyzing these vibrational modes, it becomes possible to remotely tune interfacial water behavior. Based on the spectrum analysis of the ordered water structures, we introduced a theoretical framework for terahertz modulation[115,116] aiming to remotely and controllably manipulate surface properties using external electric fields. Notably, on typical hydrophilic face-center cubic (FCC) surface with crystal face of 100, we observed characteristic far-infrared peaks near 32.9 THz,[115] corresponding to vibrational modes not found in bulk water. This led to a novel strategy by applying an external field around 32.9 THz that can trigger a phase transition in the interfacial layer from ordered to disordered states (Fig. 7). Thus, the wetting transition from hydrophobicity to hydrophilicity occurred. Upon application of a 32.9 THz electromagnetic field, the rotational and vibrational kinetic energy (ΔE_{R-V}) of water molecules exhibited a rapid and significant increase, while the translational kinetic energy (ΔE_T) rose more gradually. The effectiveness of this approach stems from the selective energy transfer into rotational and vibrational modes of the interfacial water layer. Once the water molecules acquire sufficient rotational energy, the hydrogen bonds between them are disrupted, leading to an order–disorder phase transition of the interface water. This resonant coupling effectively alters wettability, representing a promising advancement in electrowetting technologies.

In a similar context, it is recognized that in interfacial heterogeneous catalysis, gas-phase reactants must pass through the interfacial water layer to access catalytic sites — this step is essential in determining overall reaction rates. By analyzing the vibrational modes of structured interfacial water, it becomes possible to use targeted electromagnetic fields that can penetrate bulk water without causing thermal disturbances, thereby selectively tuning the configuration and dynamics of the ordered water monolayer at the interface[116] (Fig. 8). This targeted excitation induces a structural shift from an ordered to a more disordered state, which in turn reduces the barrier for oxygen molecules to approach the metal catalyst surface at ambient conditions. Theoretically, this mechanism offers a substantial boost to the performance of oxygen reduction reactions (ORR), a finding that has been corroborated by experimental results. This non-thermal, frequency-specific strategy introduces a new direction for promoting redox catalysis by precisely regulating the physical state of interfacial water.

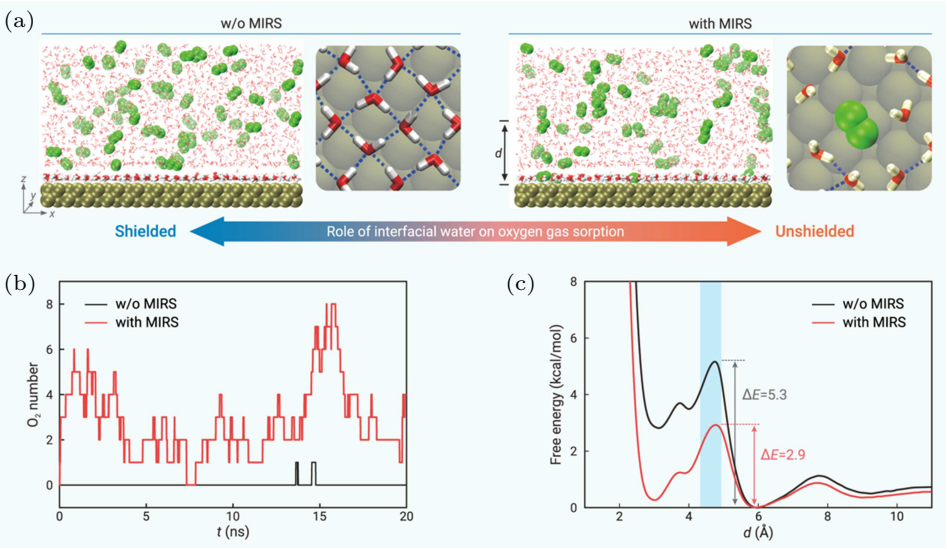


Fig. 8. Enhanced O_2 adsorption on Pt(100) induced by mid-infrared stimulation (MIRS) at 1000 cm^{-1}. (a) Side and top perspectives illustrate the adsorption configurations of water molecules (red and white) and oxygen on a Pt(100) surface, comparing cases with and without mid-infrared excitation. (b) Time evolution of adsorbed O_2 molecule count on the Pt(100) surface throughout the simulation. Red and black lines indicate results from simulations performed with and without MIRS, respectively. (c) Free energy landscape of oxygen molecules approaching the Pt(100) surface in aqueous environments, with the red curve representing conditions under MIRS and the black curve denoting the control without stimulation.

In addition, simulation studies have reported that THz waves can accelerate the unwinding of the DNA double helix.[117,118] In confined water systems, such as water confined within carbon nanotubes, THz waves have been shown to induce hydrogen bond vibrations via resonance, triggering a phase transition from an ice-like state to a super-permeable or quasi-gaseous state. This transition enhances water transport efficiency and improves nanofluidic performance.[107,119–121] Excitingly, experimental research in 2021 marked a breakthrough in THz wave modulation of neural behavior. Using two-photon calcium imaging and related methods, Chen *et al.* revealed that exposure to THz waves leads to increased

neuronal activation in the mouse cerebral cortex, resulting in improved learning performance.[122] Shu *et al.* provided the first experimental evidence that electromagnetic stimulation at 53.7 THz can remotely modulate action potentials in neural cells through a non-thermal mechanism, ultimately enabling behavioral control in animals.[123] These findings underscore the tremendous potential of THz waves in modulating the structure and properties of interfacial water. By significantly influencing water organization and diffusion behavior, THz technology holds great promise for applications in surface water and ice control, catalytic reactions, biomedicine, and nanotechnology.

5. Conclusion

This review systematically summarizes the phase transition behaviors of interfacial water and its functional roles across physical, chemical, and biological systems. Based on molecular dynamics simulations, we have for the first time predicted the phenomenon with a water droplet on a water monolayer under ambient conditions, termed as "ordered water monolayers that do not completely wet water". This water monolayer exhibits a hexagonal monolayer ice-like structure and hydrogen bond network. The specific arrangement of positive and negative ions on the substrate induces a transition of interfacial water from a disordered to an ordered phase on the ionic surface with appropriate lattice constant. On certain solid surfaces, including metals, metal oxides, polymers, and self-assembled monolayers, water molecules can form similar highly ordered structures and water droplet on this monolayer. The order–disorder phase transition of interfacial water also significantly affects ice nucleation processes. The Janus effect exhibited by AFPs highlights the molecular-level role of interfacial water ordering in modulating nucleation: NIBF suppresses nucleation by disrupting the hydrogen-bond network, whereas the IBF promotes the formation of a three-dimensional ice nucleus through geometric matching and cooperative hydrogen bonding. Fully atomic molecular dynamics simulations further demonstrate that directionally confined water molecules on the IBF can substantially lower the free energy barrier for ice nucleation. We also highlight recent advances in frequency-dependent external field modulation of the interfacial water phase transition, particularly the application of THz electromagnetic fields to precisely control the rotational and vibrational degrees of freedom of interfacial water molecules without introducing thermal effects. This THz strategy not only provides a novel physical approach to modulating surface wettability, but also successfully enhance the catalytic activity in ORR. Despite significant progresses, the challenges in the phase transitions of ordered interfacial or confined water or aqueous structures need deeper theorical investigations at the molecular level. These studies closely relate to the surface catalysis, anti-freeze materials, water-based transistors, disease treatment and drug delivery applications.

Acknowledgements

This work was supported by the National Natural Science Foundation of China (Grant Nos. 22576126, 12074394, and 12022508). We are also thankful for the computing resources and technical support provided by Shanghai Snowlake Technology Co. Ltd. and the Shanghai Supercomputing Center.

References

[1] Ben-Naim A 2011 *J. Chem. Phys.* **135** 085104
[2] Xu L, Kumar P, Buldyrev S V, Chen S H, Poole P H, Sciortino F and Stanley H E 2005 *Proc. Natl. Acad. Sci. USA* **102** 16558
[3] Shi R and Tanaka H 2020 *Proc. Natl. Acad. Sci. USA* **117** 26591
[4] Koga K, Zeng X C and Tanaka H 1997 *Phys. Rev. Lett.* **79** 5262
[5] Koga K, Tanaka H and Zeng X C 2000 *Nature* **408** 564
[6] Algara-Siller G, Lehtinen O, Wang F C, Nair R R, Kaiser U, Wu H A, Geim A K and Grigorieva I V 2015 *Nature* **519** 443
[7] Hummer G, Rasaiah J C and Noworyta J P 2001 *Nature* **414** 188
[8] Bai G, Gao D, Liu Z, Zhou X and Wang J 2019 *Nature* **576** 437
[9] Wang Y H, Zheng S, Yang W M, Zhou R Y, He Q F, Radjenovic P, Dong J C, Li S, Zheng J, Yang Z L, Attard G, Pan F, Tian Z Q and Li J F 2021 *Nature* **600** 81
[10] Litman Y, Chiang K Y, Seki T, Nagata Y and Bonn M 2024 *Nat. Chem.* **16** 644
[11] Ball P 2008 *Chemphyschem* **9** 2677
[12] Ball P 2017 *Proc. Natl. Acad. Sci. USA* **114** 13327
[13] Pal S K and Zewail A H 2004 *Chem. Rev.* **104** 2099
[14] Lv J, Song Y, Jiang L and Wang J 2014 *Acs Nano* **8** 3152
[15] Dolev M B, Braslavsky I and Davies P L 2016 *Annu. Rev. Biochem.* **85** 515
[16] Esfandiar A, Radha B, Wang F C, Yang Q, Hu S, Garaj S, Nair R R, Geim A K and Gopinadhan K 2017 *Science* **358** 511
[17] Chen L, Shi G, Shen J, Peng B, Zhang B, Wang Y, Bian F, Wang J, Li D, Qian Z, Xu G, Liu G, Zeng J, Zhang L, Yang Y, Zhou G, Wu M, Jin W, Li J and Fang H 2017 *Nature* **550** 380
[18] Gröger H, Gallou F and Lipshutz B H 2023 *Chem. Rev.* **123** 5262
[19] Guo Q, Ma Z, Zhou C, Ren Z and Yang X 2019 *Chem. Rev.* **119** 11020
[20] Hu C, Dong Y, Shi Q, Long R and Xiong Y 2025 *Chem. Soc. Rev.* **54** 524
[21] Li H, Fang W, Wang L X, Liu Y, Liu L, Sun T, Liao C, Zhu Y, Wang L and Xiao F S 2023 *The Innovation* **4** 100445
[22] Liu Z, Sinopoli A, Francisco J S and Gladich I 2024 *J. Am. Chem. Soc.* **146** 17898
[23] Wang D, Sheng T, Chen J, Wang H F and Hu P 2018 *Nat. Catal.* **1** 291
[24] Xiong H, Kunwar D, Jiang D, García-Vargas C E, Li H, Du C, Canning G, Pereira-Hernandez X I, Wan Q, Lin S, Purdy S C, Miller J T, Leung K, Chou S S, Brongersma H H, Ter Veen R, Huang J, Guo H, Wang Y and Datye A K 2021 *Nat. Catal.* **4** 830
[25] Bañuelos J L, Borguet E, Brown G E, Jr., Cygan R T, Deyoreo J J, Dove P M, Gaigeot M P, Geiger F M, Gibbs J M, Grassian V H, Ilgen A G, Jun Y S, Kabengi N, Katz L, Kubicki J D, Lützenkirchen J, Putnis C V, Remsing R C, Rosso K M, Rother G, Sulpizi M, Villalobos M and Zhang H 2023 *Chem. Rev.* **123** 6413
[26] Sposito G, Skipper N T, Sutton R, Park S H, Soper A K and Greathouse J A 1999 *Proc. Natl. Acad. Sci. USA* **96** 3358
[27] Hamm L M, Bourg I C, Wallace A F and Rotenberg B 2013 *Rev. Mineral Geochem.* **77** 189
[28] Li J, Ha N S, Liu T L, Van Dam R M and Kim C J 2019 *Nature* **572** 507
[29] Squires T M and Quake S R 2005 *Rev. Mod. Phys.* **77** 977
[30] Lohse D and Zhang X 2015 *Rev. Mod. Phys.* **87** 981
[31] Koga K, Gao G T, Tanaka H and Zeng X C 2001 *Nature* **412** 802
[32] Wan R, Li J, Lu H and Fang H 2005 *J. Am. Chem. Soc.* **127** 7166
[33] Li J Y, Gong X J, Lu H J, Li D, Fang H P and Zhou R H 2007 *Proc. Natl. Acad. Sci. USA* **104** 3687

[34] Fang H, Wan R and Li S 2008 *J. Phys. D: App. Phys.* **41** 103002
[35] Hu J, Xiao X D, Ogletree D F and Salmeron M 1995 *Science* **268** 267
[36] Odelius M, Bernasconi M and Parrinello M 1997 *Phys. Rev. Lett.* **78** 2855
[37] Miranda P B, Xu L, Shen Y R and Salmeron M 1998 *Phys. Rev. Lett.* **81** 5876
[38] Ogasawara H, Brena B, Nordlund D, Nyberg M, Pelmenschikov A, Pettersson L G M and Nilsson A 2002 *Phys. Rev. Lett.* **89** 276102
[39] Feibelman P J 2002 *Science* **295** 99
[40] Meng S, Xu L F, Wang E G and Gao S W 2002 *Phys. Rev. Lett.* **89** 176104
[41] Giovambattista N, Rossky P J and Debenedetti P G 2009 *Phys. Rev. Lett.* **102** 050603
[42] Han S H, Choi M Y, Kumar P and Stanley H E 2010 *Nat. Phys.* **6** 685
[43] Guo J, Meng X, Chen J, Peng J, Sheng J, Li X Z, Xu L, Shi J R, Wang E and Jiang Y 2014 *Nat. Mater.* **13** 184
[44] Ma R, Cao D, Zhu C, Tian Y, Peng J, Guo J, Chen J, Li X Z, Francisco J S, Zeng X C, Xu L M, Wang E G and Jiang Y 2020 *Nature* **577** 60
[45] Wu D, Zhao Z, Lin B, Song Y, Qi J, Jiang J, Yuan Z, Cheng B, Zhao M, Tian Y, Wang Z, Wu M, Bian K, Liu K H, Xu L M, Zeng X C, Wang E G and Jiang Y 2024 *Science* **384** 1254
[46] Wang Z, Yuan Z, Cheng M, Huang X, Liu K, Wang Y, Sun H, Liao L, Xu Z, Chen J, Wang W, Liu L, Bai X, Xu L, Wang E and Wang L 2025 *Nat. Commun.* **16** 7349
[47] Kapil V, Schran C, Zen A, Chen J, Pickard C J and Michaelides A 2022 *Nature* **609** 512
[48] Jiang J, Gao Y, Li L, Liu Y, Zhu W, Zhu C, Francisco J S and Zeng X C 2024 *Nat. Phys.* **20** 456
[49] Wang C L, Lu H J, Wang Z G, Xiu P, Zhou B, Zuo G H, Wan R Z, Hu J and Fang H P 2009 *Phys. Rev. Lett.* **103** 137801
[50] Wang C, Qi C, Tu Y, Nie X and Liang S 2019 *Phys. Rev. Mater.* **3** 065602
[51] Guo P, Tu Y S, Yang J R, Wang C L, Sheng N and Fang H P 2015 *Phys. Rev. Lett.* **115** 186101
[52] James M, Darwish T A, Ciampi S, Sylvester S O, Zhang Z, Ng A, Gooding J J and Hanley T L 2011 *Soft Matt.* **7** 5309
[53] Qu M, Huang G, Liu X, Nie X, Qi C, Wang H, Hu J, Fang H, Gao Y, Liu W T, Francisco J S and Wang C 2022 *Chem. Sci.* **13** 10546
[54] Agosta L, Arismendi D, Dzugutov M and Hermansson K 2023 *Angew. Chem. Int. Ed.* **62** e202303910
[55] Limmer D T, Willard A P, Madden P and Chandler D 2013 *Proc. Natl. Acad. Sci. USA* **110** 4200
[56] Xu Z, Gao Y, Wang C L and Fang H P 2015 *J. Phys. Chem. C* **119** 20409
[57] Argyris D, Ho T, Cole D R and Striolo A 2011 *J. Phys. Chem. C* **115** 2038
[58] Wang Y, Duan Z and Fan D 2013 *Sci. Rep.* **3** 3505
[59] Rotenberg B, Patel A J and Chandler D 2011 *J. Am. Chem. Soc.* **133** 20521
[60] Zhang J, Tan J, Pei R, Ye S and Luo Y 2021 *J. Am. Chem. Soc.* **143** 13074
[61] Bista I, Wood J M D, Desvignes T, Mccarthy S A, Matschiner M, Ning Z, Tracey A, Torrance J, Sims Y, Chow W, Smith M, Oliver K, Haggerty L, Salzburger W, Postlethwait J H, Howe K, Clark M S, William Detrich H, Christina Cheng C H, Miska E A and Durbin R 2023 *Nat. Commun.* **14** 3412
[62] Liou Y C, Tocilj A, Davies P L and Jia Z 2000 *Nature* **406** 322
[63] Sicheri F and Yang D S 1995 *Nature* **375** 427
[64] Marshall C B, Fletcher G L and Davies P L 2004 *Nature* **429** 153
[65] Tas R P, Hendrix M M R M and Voets I K 2023 *Proc. Natl. Acad. Sci. USA* **120** e2212456120
[66] Bar Dolev M, Braslavsky I and Davies P L 2016 *Annu. Rev. Biochem.* **85** 515
[67] Yeh Y and Feeney R E 1996 *Chem. Rev.* **96** 601
[68] Zhang X, Yang J, Tian Y and Zhang L 2025 *J. Am. Chem. Soc.* **147** 17682
[69] Liu Z, Zheng X and Wang J 2022 *J. Am. Chem. Soc.* **144** 5685
[70] Fu Y, Li Y, Liu S and Chen J 2025 *Trends Food Sci. Technol.* **164** 105252
[71] Eickhoff L, Dreischmeier K, Zipori A, Sirotinskaya V, Adar C, Reicher N, Braslavsky I, Rudich Y and Koop T 2019 *Phys. Chem. Lett.* **10** 966
[72] Liu K, Wang C, Ma J, Shi G, Yao X, Fang H, Song Y and Wang J 2016 *Proc. Natl. Acad. Sci. USA* **113** 14739
[73] Fitzner M, Sosso G C, Cox S J and Michaelides A 2015 *J. Am. Chem. Soc.* **137** 13658
[74] Algara-Siller G, Lehtinen O, Wang F C, Nair R R, Kaiser U, Wu H A, Geim A K and Grigorieva I V 2015 *Nature* **519** 443
[75] Jiang J, Gao Y, Li L, Liu Y, Zhu W, Zhu C, Francisco J S and Zeng X C 2024 *Nat. Phys.* **20** 456
[76] Murray B J, O'sullivan D, Atkinson J D and Webb M E 2012 *Chem. Soc. Rev.* **41** 6519
[77] He Z and Wang J 2022 *The Innovation* **3** 100287
[78] Tang M, Cziczo D J and Grassian V H 2016 *Chem. Rev.* **116** 4205
[79] Hudait A, Odendahl N, Qiu Y, Paesani F and Molinero V 2018 *J. Am. Chem. Soc.* **140** 4905
[80] Hudait A, Moberg D R, Qiu Y, Odendahl N, Paesani F and Molinero V 2018 *Proc. Natl. Acad. Sci. USA* **115** 8266
[81] Cui J, Battle K, Wierzbicki A and Madura J D 2009 *Int. J. Quantum Chem.* **109** 73
[82] Nutt D R and Smith J C 2008 *J. Am. Chem. Soc.* **130** 13066
[83] Meister K, Ebbinghaus S, Xu Y, Duman J G, Devries A, Gruebele M, Leitner D M and Havenith M 2013 *Proc. Natl. Acad. Sci. USA* **110** 1617
[84] Midya U S and Bandyopadhyay S 2025 *Adv. Theor. Simul.* **8** 2400642
[85] Lupi L, Hudait A, Peters B, Grünwald M, Gotchy Mullen R, Nguyen A H and Molinero V 2017 *Nature* **551** 218
[86] Qiu Y, Odendahl N, Hudait A, Mason R, Bertram A K, Paesani F, Demott P J and Molinero V 2017 *J. Am. Chem. Soc.* **139** 3052
[87] Hudait A, Moberg D R, Qiu Y, Odendahl N, Paesani F and Molinero V 2018 *Proc. Natl. Acad. Sci. USA* **115** 8266
[88] Zhang Y, Wei N, Li L, Liu Y, Huang C, Li Z, Huang Y, Zhang D, Francisco J S, Zhao J, Wang C and Zeng X C 2025 *J. Am. Chem. Soc.* **147** 4411
[89] Sosso G C, Chen J, Cox S J, Fitzner M, Pedevilla P, Zen A and Michaelides A 2016 *Chem. Rev.* **116** 7078
[90] Zhang Y, Wei N, Li L, Liu Y, Huang C, Li Z, Huang Y, Zhang D, Francisco J S, Zhao J, Wang C and Zeng X C 2025 *J. Am. Chem. Soc.* **147** 4411
[91] Michaelides A and Morgenstern K 2007 *Nat. Mater.* **6** 597
[92] Cox S J, Kathmann S M, Slater B and Michaelides A 2015 *J. Chem. Phys.* **142** 184704
[93] Zhang H, Du H, Zhu D, Zhao H, Zhang X, He F, Wang L, Lv C and Hao P 2024 *ACS Appl. Mater. Interfaces* **16** 11084
[94] Lupi L, Hudait A and Molinero V 2014 *J. Am. Chem. Soc.***136** 3156
[95] Liu J, Zhu C, Liu K, Jiang Y, Song Y, Francisco J S, Zeng X C and Wang J 2017 *Proc. Natl. Acad. Sci. USA* **114** 11285
[96] Qiu H and Guo W 2019 *J. Phys. Chem. Lett.* **10** 6316
[97] Lupi L and Molinero V 2014 *J. Phys. Chem. A* **118** 7330
[98] Bi Y, Cabriolu R and Li T 2016 *J. Phys. Chem. C* **120** 1507
[99] Davies M B, Fitzner M and Michaelides A 2022 *Proc. Natl. Acad. Sci. USA* **119** e2205347119
[100] Fu X and Zhou X 2023 *Chin. Phys. B* **32** 28202
[101] Zhang C, Wang Y, Wang J and Zhou X 2022 *J. Phys. Chem. C* **126** 13373
[102] Zielke S A, Bertram A K and Patey G N 2015 *J. Phys. Chem. B* **119** 9049
[103] Huang Y, Liang W, Huang L, Zhang Y, Yang H, Wei N, Wang C and Sun Z 2024 *J. Mol. Liq.* **412** 125854
[104] Sun G and Tanaka H 2025 *J. Colloid Interface Sci.* **698** 137812
[105] Savolainen J, Ahmed S and Hamm P 2013 *Proc. Natl. Acad. Sci. USA* **110** 20402
[106] Elgabarty H, Kampfrath T, Bonthuis D J, Balos V, Kaliannan N K, Loche P, Netz R R, Wolf M, Kühne T D and Sajadi M 2020 *Sci. Adv.* **6** eaay7074
[107] Zhu Z, Chang C, Shu Y and Song B 2020 *J. Phys. Chem. Lett.* **11** 256
[108] Tonouchi M 2007 *Nat. Photonics* **1** 97
[109] Fattinger C and Grischkowsky D 1989 *Appl. Phys. Lett.* **54** 490
[110] Schmuttenmaer C A 2004 *Chem. Rev.* **104** 1759
[111] Siegel P H 2002 *IEEE Trans. Microwave Theory Tech.* **50** 910

[112] Carletti L, Mcdonnell C, Arregui Leon U, Rocco D, Finazzi M, Toma A, Ellenbogen T, Della Valle G, Celebrano M and De Angelis C 2023 *ACS Photonics* **10** 3419

[113] Carr G L, Martin M C, Mckinney W R, Jordan K, Neil G R and Williams G P 2002 *Nature* **420** 153

[114] Gopal A, Herzer S, Schmidt A, Singh P, Reinhard A, Ziegler W, Brömmel D, Karmakar A, Gibbon P, Dillner U, May T, Meyer H G and Paulus G G 2013 *Phys. Rev. Lett.* **111** 074802

[115] Zhu Z, Zhu J, Chang C, Qi C, Zhu Z, Zhao H, Zhang D, Zeng X C and Wang C 2024 *Nano Lett.* **24** 3243

[116] Zhang Q, Wu Y, Sun H, Zhu Z, Zhao H, Yang J, Wang J, Chen M, Song S, Zheng S, Zhang D, Yang H, Zhu Z and Wang C 2025 *The Innovation* **6** 100754

[117] Yuan Y, Lou J, Wu K, Yu Y, Li C, Peng W, Han Y, Li J and Chang C 2024 *ACS Photonics* **11** 1473

[118] Zhang C, Yuan Y, Wu K, Wang Y, Zhu S, Shi J, Wang L, Li Q, Zuo X, Fan C, Chang C and Li J 2022 *Nano Lett.* **22** 468

[119] Kou J, Lu H, Wu F, Fan J and Yao J 2014 *Nano Lett.* **14** 4931

[120] Zhang Q L, Jiang W Z, Liu J, Miao R D and Sheng N 2013 *Phys. Rev. Lett.* **110** 254501

[121] Zhang Q L, Yang R Y, Jiang W Z and Huang Z Q 2016 *Nanoscale* **8** 1886

[122] Zhang J, He Y, Liang S, Liao X, Li T, Qiao Z, Chang C, Jia H and Chen X 2021 *Nat. Commun.* **12** 2730

[123] Liu X, Qiao Z, Chai Y, Zhu Z, Wu K, Ji W, Li D, Xiao Y, Mao L, Chang C, Wen Q, Song B and Shu Y 2021 *Proc. Natl. Acad. Sci. USA* **118** e2015685118